Supplemental information for:

The higher plant plastid NAD(P)H dehydrogenase-like complex (NDH) is a high efficiency proton pump that increases ATP production by cyclic electron flow

Deserah D. Strand[1,*], Nicholas Fisher[1,*], and David M. Kramer[1,2]

[1]MSU-DOE Plant Research Laboratory, [2]Biochemistry, Michigan State University, East Lansing, MI 48823

Figure S1. Pathways of linear- and cyclic electron flow in the thylakoid membrane

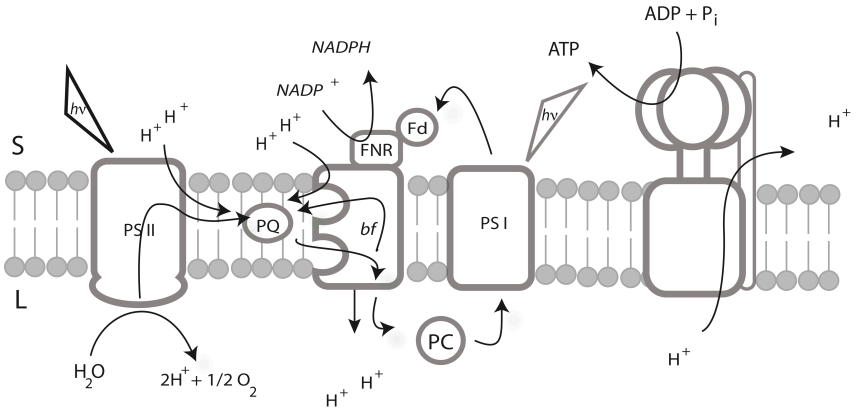

A

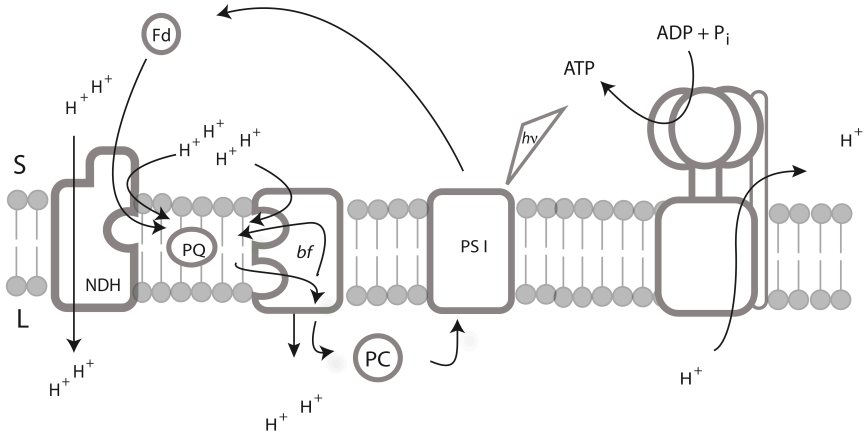

B

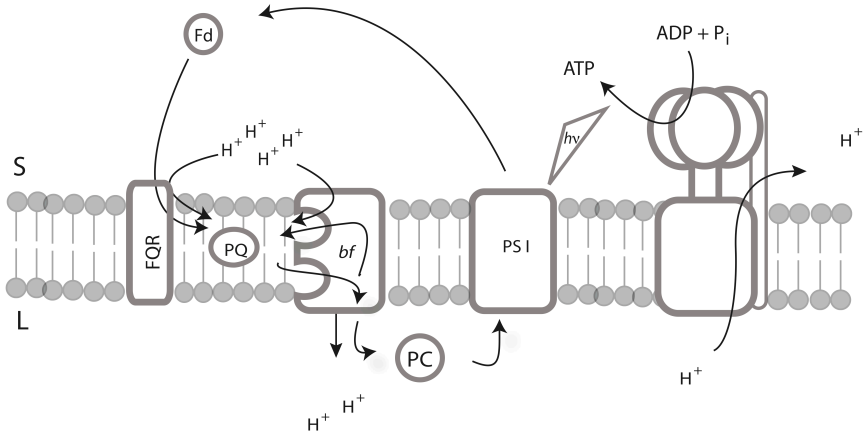

C

Fig. S1. Electron and proton transfer pathways in plant thylakoids. A) Linear electron flow. Electrons are extracted from water, and passed through photosystem II (PS II) to plastoquinone (PQ), the cytochrome *bf* complex (*bf*), plastocyanin (PC), photosystem I (PS I), and finally to ferredoxin (Fd), which can further reduce $NADP^+$ via the ferredoxin:nadp reductase (FNR). Protons (H^+) are deposited in the lumen at PS II and during plastoquinol oxidation at the *bf* complex. B) Cyclic electron flow involving a proton-pumping NADPH dehydrogenase complex (NDH). Electrons are donated to NDH via Fd and are passed to PQ, the *bf* complex, PS I, and finally back to Fd. Protons are deposited in the lumen by NDH and during plastoquinol oxidation at the *bf* complex. C) CEF involving the ferredoxin:quinone reductase (FQR). Electrons are donated to FQR via Fd and are passed to PQ, the *bf* complex, PS I, and finally back to Fd. Protons are deposited in the lumen only during plastoquinol oxidation at the *bf* complex.

Figure S2. NDH membrane domain sequence alignments versus mitochondrial (ND*x*/nu*x*m) and bacterial (nqo*x*/nuo*x*) respiratory Complex I homologues. Sequence data were obtained from UniProt (www.uniprot.org, March 26, 2015 release) and aligned using ClustalW2 at ebi.ac.uk.

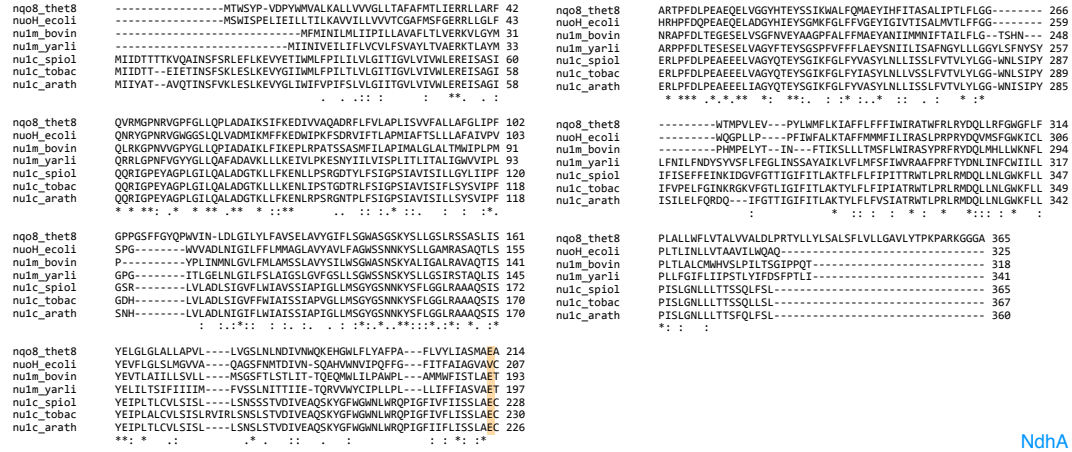

Fig. S2(A): NdhA(ND-1/NuoH/NQO8) sequence alignment. Sequences are named according to their UniProt identifiers. **NDH**: arath; *Arabidopsis thaliana*, tobac; *Nicotiana tabacum*, spiol; *Spinacia oleracea* (spinach). **Complex I**: thet8; T*hermus thermophilus*, ecoli; *Escherichia coli*, bovin; *Bos taurus* (cow), yarli; *Yarrowia lipolytica*. Conserved residues shown in Fig. 1 are highlighted in orange.

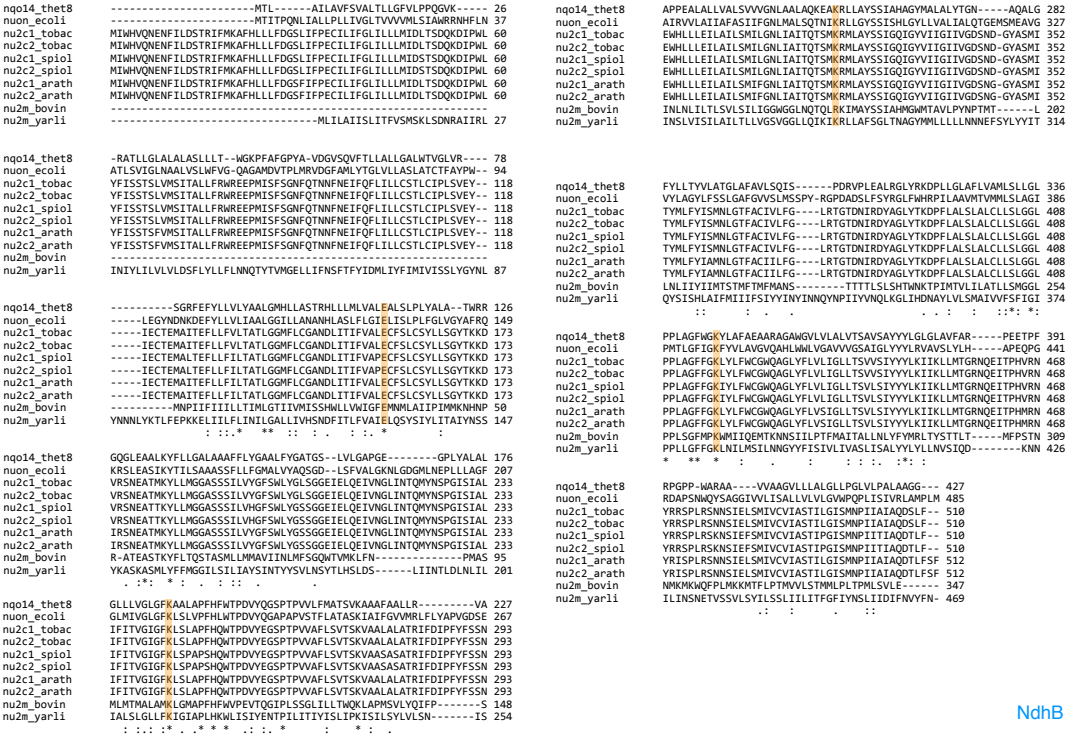

Fig. S2(B): NdhB(ND-2/NuoN/NQO14) sequence alignment. Sequences are named according to their UniProt identifiers. **NDH**: arath; *Arabidopsis thaliana*, tobac; *Nicotiana tabacum*, spiol; *Spinacia oleracea* (spinach). **Complex I**:

thet8; T*hermus thermophilus*, ecoli; *Escherichia coli*, bovin; *Bos taurus* (cow), yarli; *Yarrowia lipolytica*. Conserved residues shown in Fig. 1 are highlighted in orange. Note that NdhB is duplicated in the chloroplast genome; sequences for both NdhB and ndhb-01 are shown.

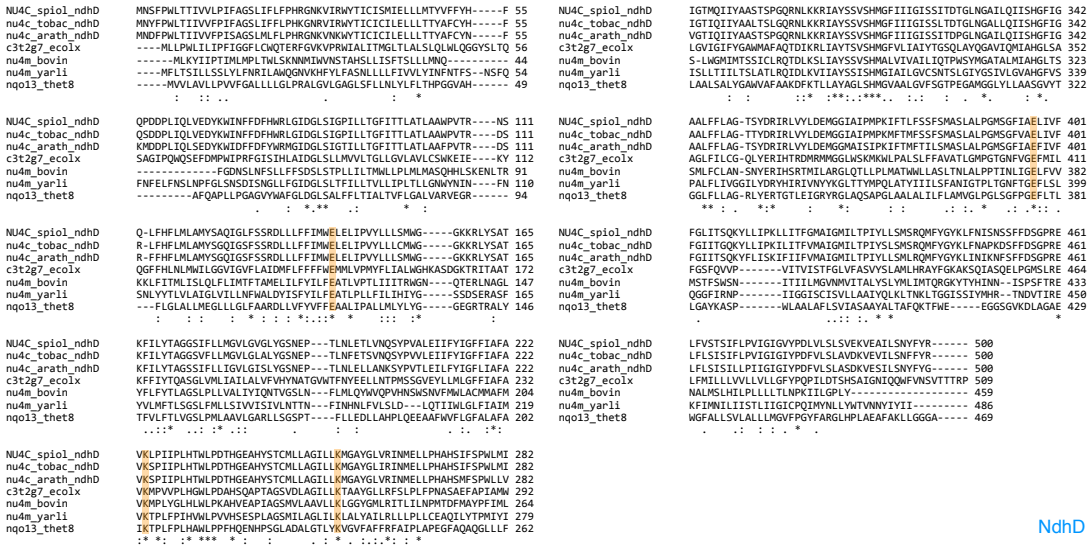

Fig. S2(C): NdhD(ND-4/NuoM/NQO13) sequence alignment. Sequences are named according to their UniProt identifiers. **NDH**: arath; *Arabidopsis thaliana*, tobac; *Nicotiana tabacum*, spiol; *Spinacia oleracea* (spinach). **Complex I**: thet8; T*hermus thermophilus*, ecolx; *Escherichia coli*, bovin; *Bos taurus* (cow), yarli; *Yarrowia lipolytica*. Conserved residues shown in Fig. 1 are highlighted in orange.

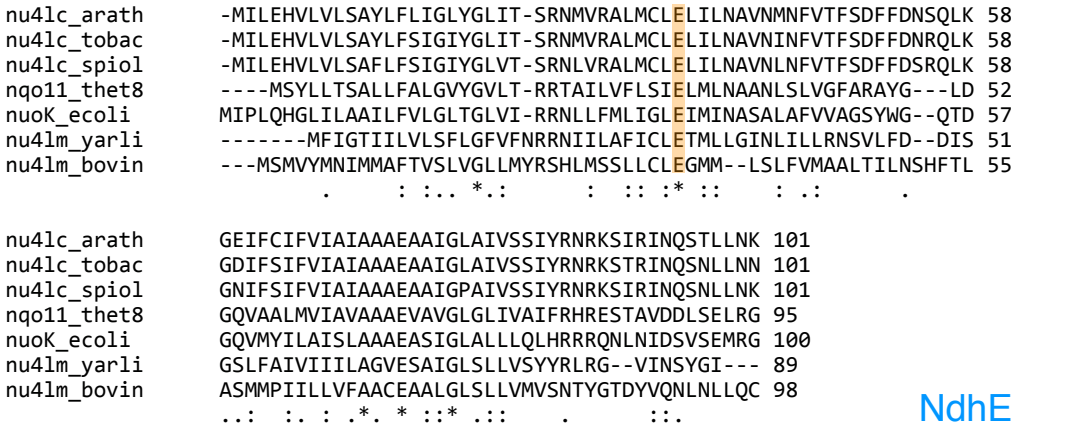

Fig. S2(D): NdhE(ND-4L/NuoK/NQO11) sequence alignment. Sequences are named according to their UniProt identifiers. **NDH:** arath; *Arabidopsis thaliana*, tobac; *Nicotiana tabacum*, spiol; *Spinacia oleracea* (spinach). **Complex I**: thet8; T*hermus thermophilus*, ecolx; *Escherichia coli*, bovin; *Bos taurus* (cow), yarli; *Yarrowia lipolytica*. Conserved residues shown in Fig. 1 are highlighted in orange.

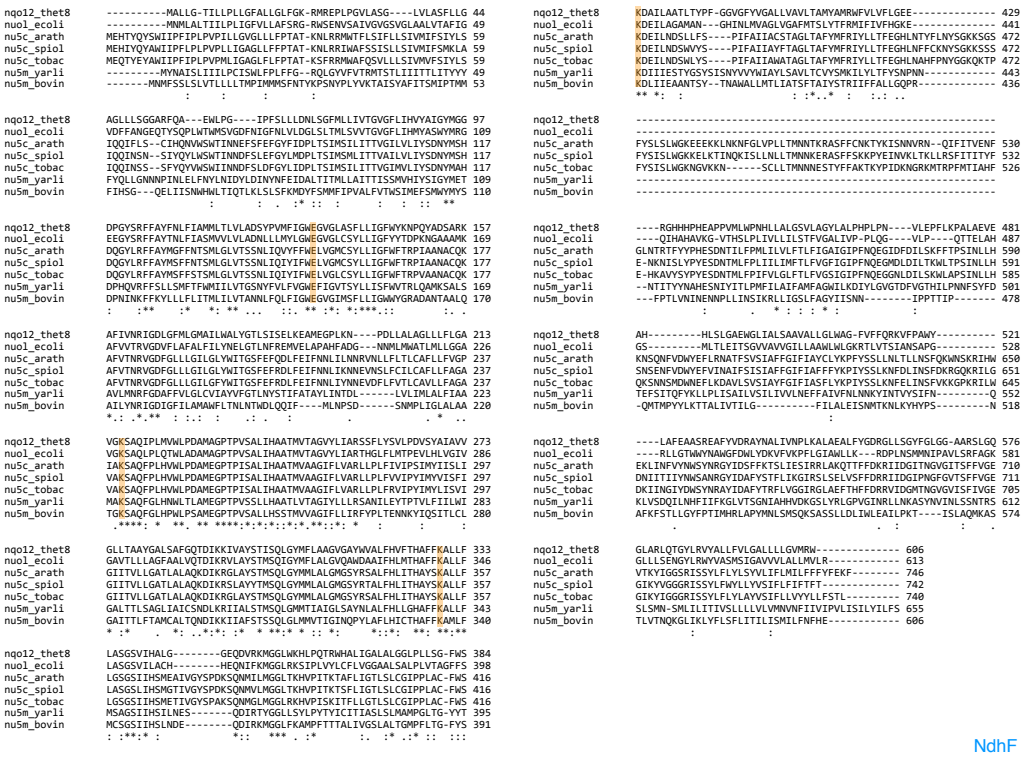

Fig. S2(E): NdhF(ND-5/NuoL/NQO12) sequence alignment. Sequences are named according to their UniProt identifiers. **NDH**: arath; *Arabidopsis thaliana*, tobac; *Nicotiana tabacum*, spiol; *Spinacia oleracea* (spinach). **Complex I**: thet8; T*hermus thermophilus*, ecolx; *Escherichia coli*, bovin; *Bos taurus* (cow), yarli; *Yarrowia lipolytica*. Conserved residues shown in Fig. 1 are highlighted in orange.

Figure S3. NDH protonmotivity assay

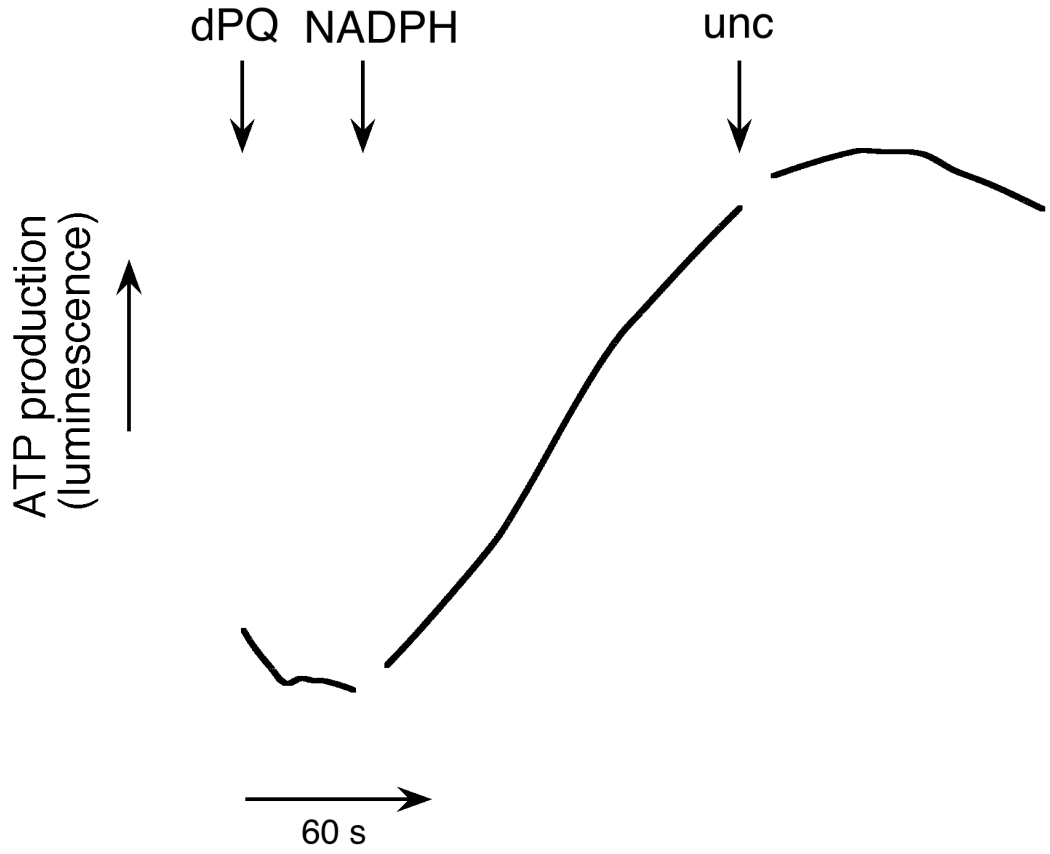

Fig. S3. ATP synthesis, monitored by luciferase luminescence, in DCMU-treated *S. oleracea* thylakoids in the dark. Assay conditions as Fig 2 unless otherwise noted. Fd was present in assay buffer at a concentration of 5 μM prior to addition of dPQ (50 μM). The reaction was initiated by the addition of 100 μM NADPH. Addition of valinomycin and nigericin (10 μM each) is indicated by 'unc'. Representative data (fitted by the locally weighted least squared error method with Kaleidagraph (Synergy Software, Reading, PA.)) are shown; discontinuities in the data are due to the removal of mixing artefacts on substrate addition.

Figure S4. Antimycin A-insensitivity of the NDH protonmotivity assay

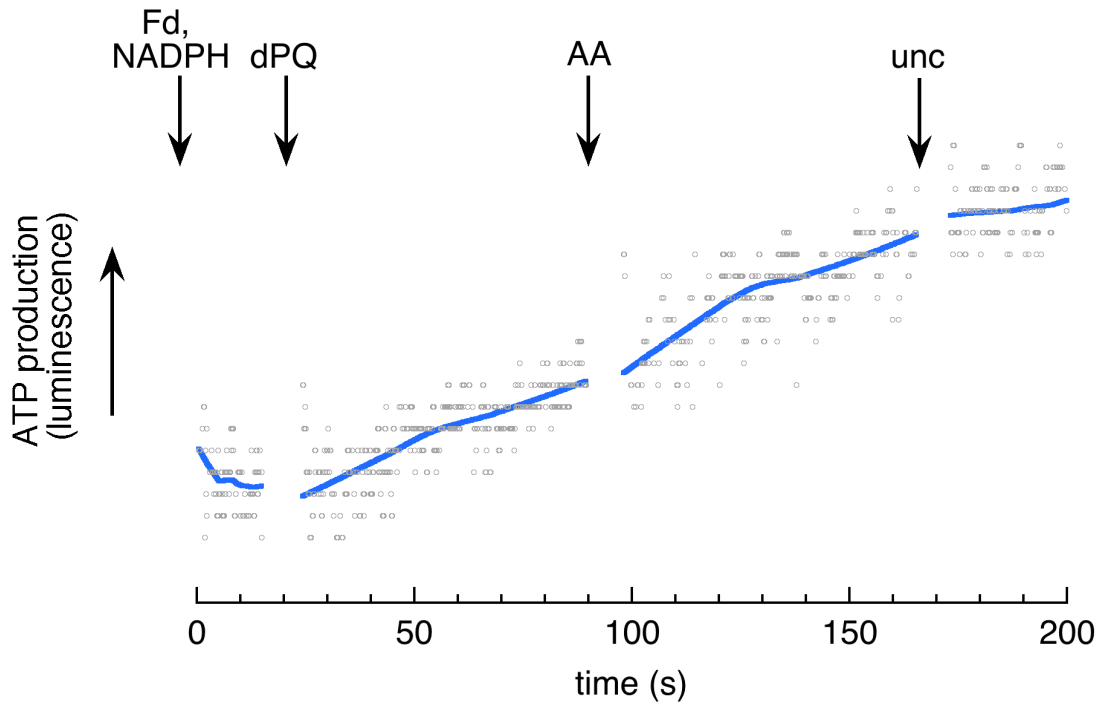

Fig. S4. ATP synthesis, monitored by luciferase luminescence, in DCMU-treated *S. oleracea* thylakoids in the dark. Assay conditions as Fig 2 unless otherwise noted. Fd and NADPH were present in assay buffer at concentrations of 5- and 100 μM respectively. The reaction was initiated by the addition of 50 μM dPQ. 10 μM antimycin A (AA) was added as indicated. Addition of valinomycin and nigericin (10 μM each) is indicated by 'unc'. Representative raw data (fitted by the locally weighted least squared error method with Kaleidagraph (Synergy Software, Reading, PA.)) are shown; discontinuities in the data are due to the removal of mixing artefacts on substrate addition.

Figure S5. The effect of tridecylstigmatellin and oligomycin on ATP generation in spinach thylakoid preparations in the dark.

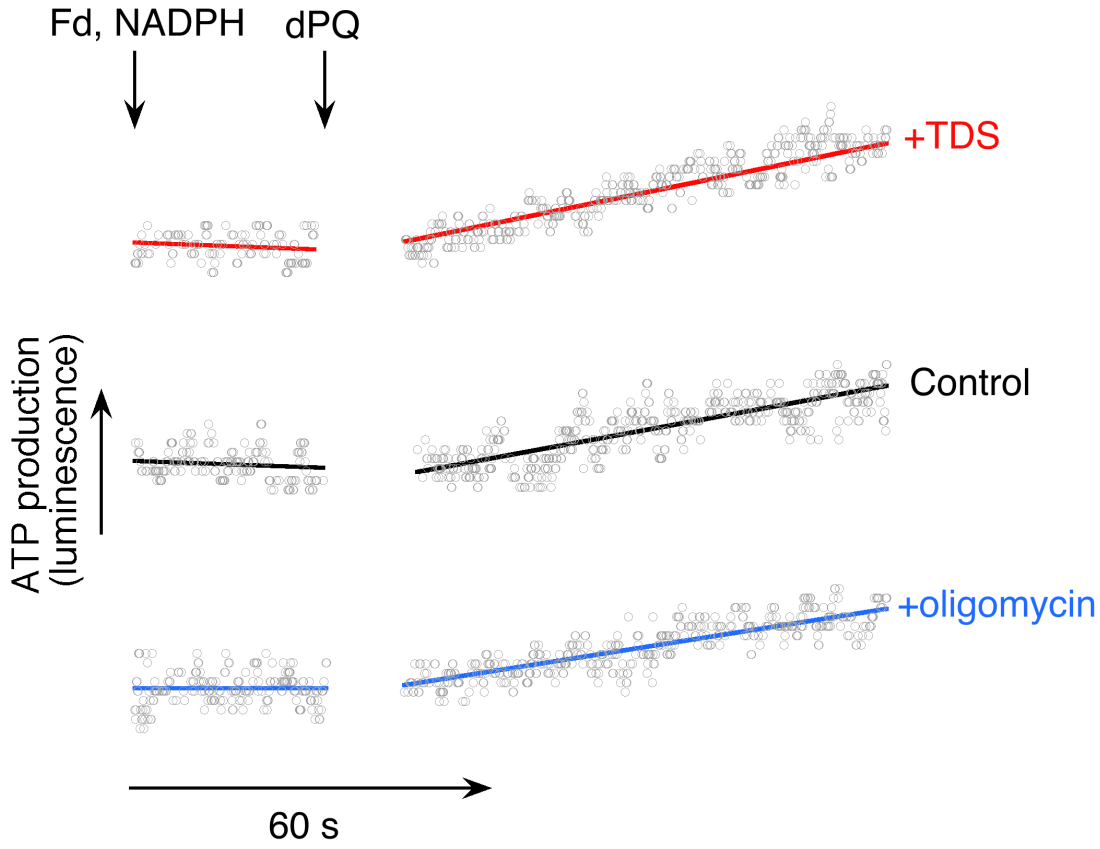

Fig. S5. ATP synthesis, monitored by luciferase luminescence, in DCMU-treated *S. oleracea* thylakoids in the dark in the presence of 1 μM tridecylstigmatellin (TDS) or 2 μM oligomycin. Fd and NADPH were present at 5- and 100 μM respectively. ATP synthesis was initiated by the addition of 50 μM decylplastoquinone (dPQ). Other conditions as in Fig. 2(D). Luminescence is reported in arbitrary units. Discontinuities in the data are due to the removal of mixing artifacts on substrate addition. Linear least squares fit to representative raw phosphoroscope data are shown. Fitting was performed using Kaleidagraph (Synergy Software, Reading, PA.). The slopes of the fits to the +TDS and +oligomycin kinetic data are 1.2- and 0.9-fold of the control respectively.

Figure S6. The effect of hydroxylamine on the post-illumination fluorescence rise in spinach thylakoid preparations

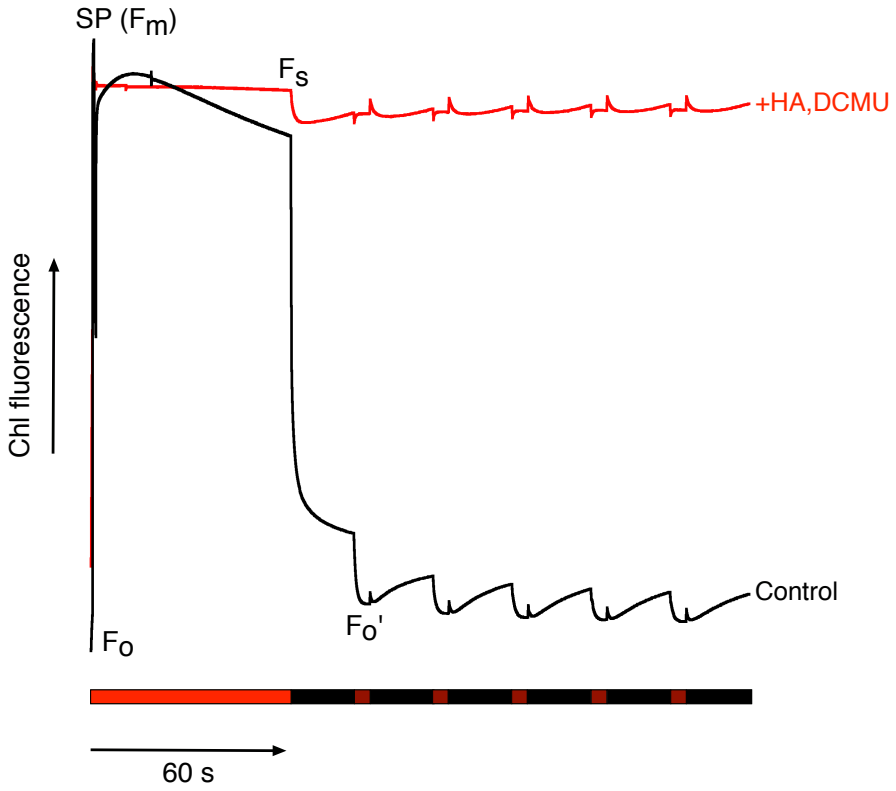

Fig. S6. The effect of hydroxylamine on the post illumination fluorescence rise in spinach thylakoid preparations. Assay conditions consisted of thylakoids suspended at 50 μg Chl/ml in 10 mM HEPES (pH 7.6), 10 mM KCl, 5 mM $MgCl_2$ supplemented with 5 μM Fd and 100 μM NADPH. Hydroxylamine (HA) and DCMU were present as indicated (red trace only) at 1 mM and 10 μM respectively. The periods of actinic- (620 nm, 250 μmol photons m^{-2} s^{-1}) and far-red (720 nm, 50 μmol photons m^{-2} s^{-1}) illumination are indicated by bright- and dark red bars under the fluorescence data. Periods of darkness are indicated by black bars. 'SP' refers to a saturating actinic flash (5000 μmol photons m^{-2} s^{-1}). F_o, F_m, F_s and F_o' indicate the fluorescence levels in the dark, during the saturating flash, during the steady state under actinic illumination and under far-red illumination respectively.

Figure S7. The effect of oxygen on the post-illumination fluorescence rise in spinach and *Amaranthus hybridus* thylakoid preparations

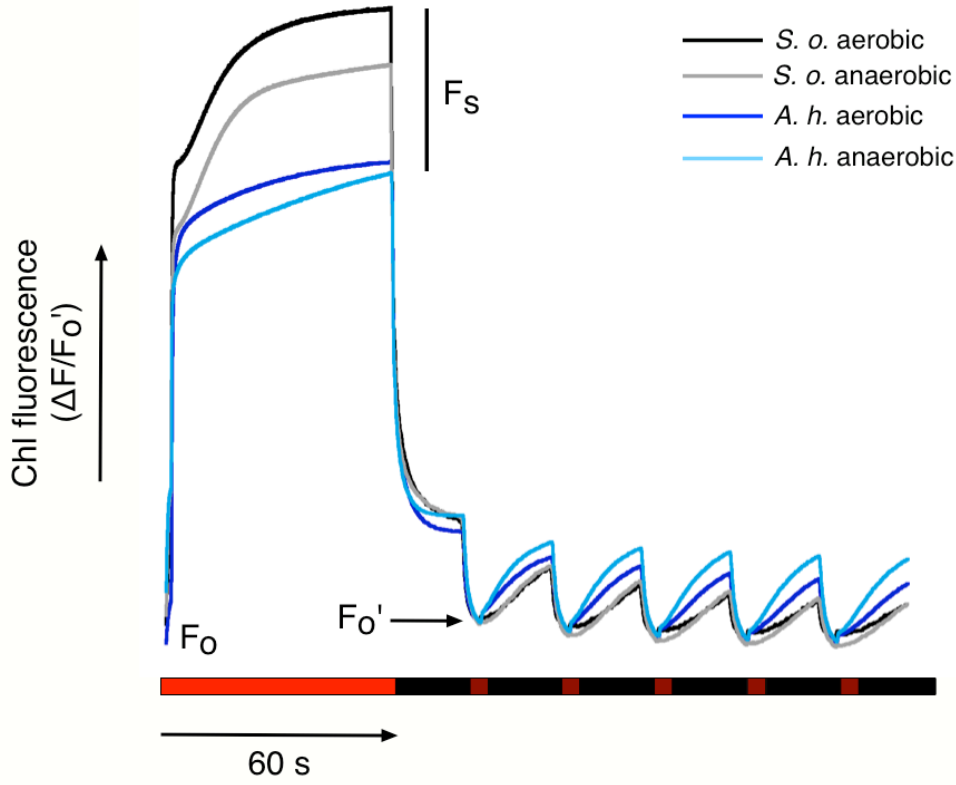

Fig. S7. The effect of oxygen on the post illumination fluorescence rise in spinach (*S.o*) thylakoid and *A. hybridus* (*A.h.*) thylakoid preparations. Assay conditions consisted of thylakoids suspended at 50 μg Chl/ml in 10 mM HEPES (pH 7.6), 10 mM KCl, 5 mM $MgCl_2$ supplemented with 5 μM Fd and 100 μM NADPH. Anaerobiosis was achieved by the addition of 10 mM glucose plus a catalytic amount of glucose oxidase to the (septum-sealed) reaction cuvette, followed by flushing with a gentle stream of nitrogen for 4 minutes. The periods of actinic- (620 nm, 250 μmol photons m^{-2} s^{-1}) and far-red (720 nm, 50 μmol photons m^{-2} s^{-1}) illumination are indicated by bright- and dark red bars under the fluorescence data. Periods of darkness are indicated by black bars. 'SP' refers to a saturating actinic flash (5000 μmol photons m^{-2} s^{-1}). F_o, F_s and F_o' indicate the fluorescence levels in the dark, during the saturating flash, during the steady state under actinic illumination and under far-red illumination respectively. A 5 point smoothing function was applied to the data, and as such the F_m point achieved during the initial saturating flash is not visible.

Figure S8. Gibbs free energy plots as a function of protonmotive force (Δp) for the oxidoreductase activity of NDH

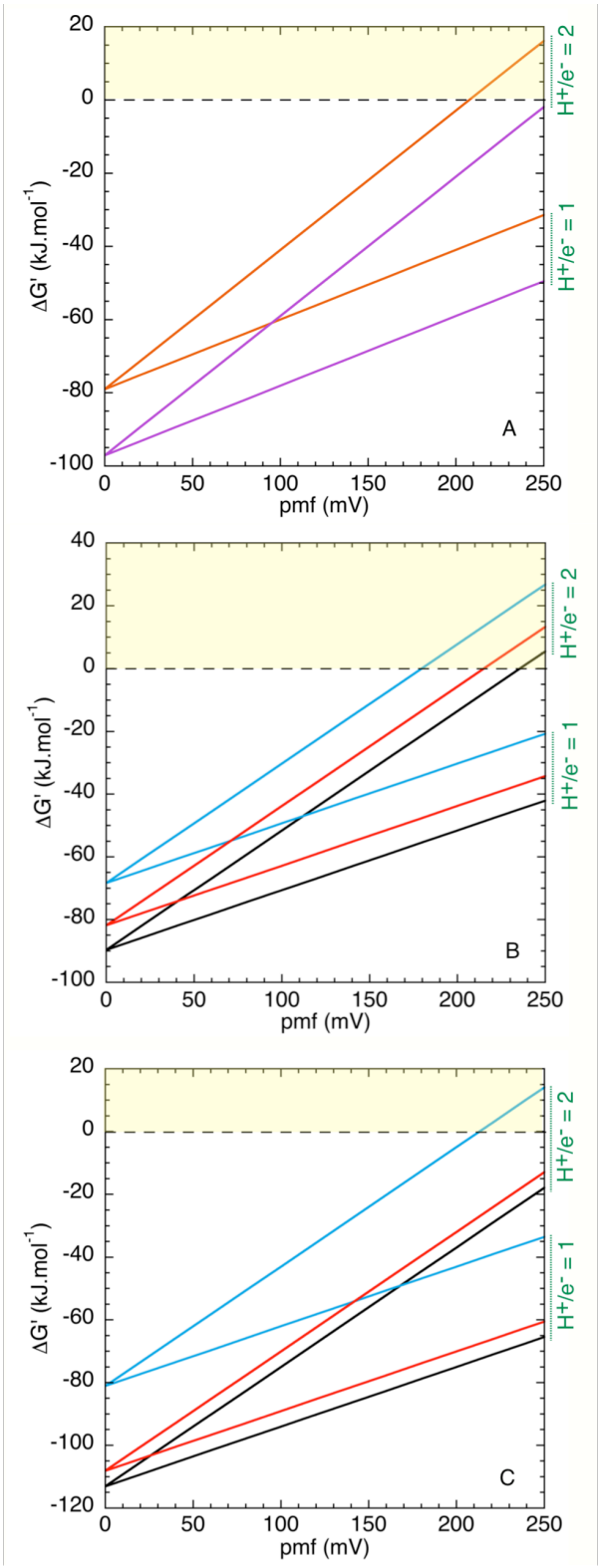

Figure S8. Gibbs free energy plots as a function of protonmotive force (Δp) for the oxidoreductase activity of NDH. Calculations were performed using equation 1 assuming a stromal pH of 7.5 and midpoint potentials ($E_{m,7.5}$) of +80, -335 and -430 mV for the PQ/PQH_2, $NADP^+$/NADPH and Fd^{3+}/Fd^{2+} couples respectively. T = 298 K. Calculated equilibrium constants (K_{eq}) were converted into Gibbs free energy values for display in Fig. 6. Yellow shaded regions indicate conditions under which the reverse (plastoquinol oxidase) reaction of NDH is energetically favorable. (A) Thermodynamics of NDH-mediated NADPH:PQ oxidoreductase (orange) and Fd:PQ oxidoreductase (purple) activity for H^+/e^- = 1 and H^+/e^- = 2 assuming 50% reduction of donors and acceptors. (B) Thermodynamics of NDH-mediated NADPH:PQ oxidoreductase activity assuming 10% reduced NADPH + 90% reduced PQH_2 (blue), 90% reduced NADPH + 90% reduced PQH_2 (red) and 90% reduced NADPH + 10% reduced PQH_2 (black) for H^+/e^- = 1 and H^+/e^- = 2. (C) Thermodynamics of NDH-mediated Fd:PQ oxidoreductase activity assuming 10% reduced Fd + 90% reduced PQH_2 (blue), 90% reduced Fd + 90% reduced PQH_2 (red) and 90% reduced Fd + 10% reduced PQH_2 (black) for H^+/e^- = 1 and H^+/e^- = 2.

$$K_{eq} = 10^{\frac{\Delta E_h - (n\Delta p)}{30}}$$ Equation 1.

Figure S9. Electrochromic shift decay kinetics

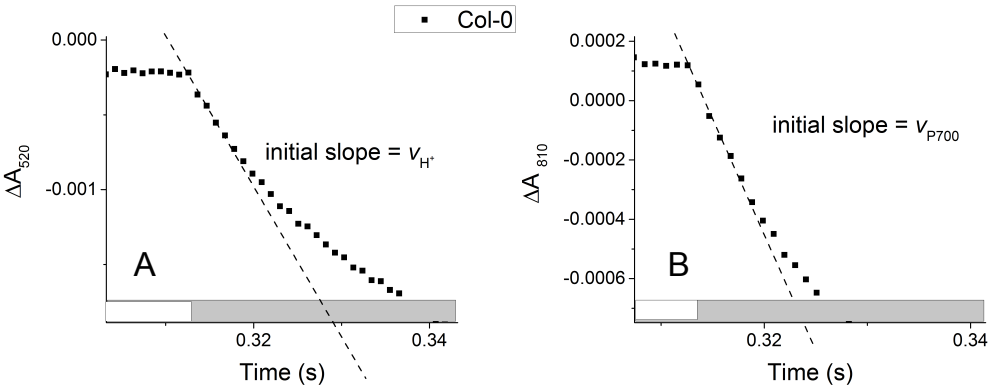

Fig. S9. Examples of analysis of raw data leading to the generation of Figure 6. A) Dark interval relaxation kinetics of absorbance at 520 nm monitoring the electrochromic shift. The initial slope of the decay is taken as the relative transthylakoid proton flux (v_H^+) parameter, which is then normalized to chlorophyll content [as described in [1–5]]. B) Dark interval relaxation kinetics of absorbance at 820 nm monitoring the reduction of $P700^+$. The initial slope of the decay is taken as the relative electron flux through P700 (v_{P700}) parameter.

Supplemental References:

1. Baker, N. R., Harbinson, J. & Kramer, D. M. Determining the limitations and regulation of photosynthetic energy transduction in leaves. *Plant. Cell Environ.* **30,** 1107–25 (2007).

2. Livingston, A. K., Kanazawa, A., Cruz, J. a & Kramer, D. M. Regulation of cyclic electron flow in C(3) plants: differential effects of limiting photosynthesis at ribulose-1,5-bisphosphate carboxylase/oxygenase and glyceraldehyde-3-phosphate dehydrogenase. *Plant. Cell Environ.* **33,** 1779–88 (2010).

3. Livingston, A. K., Cruz, J. A, Kohzuma, K., Dhingra, A. & Kramer, D. M. An Arabidopsis mutant with high cyclic electron flow around photosystem I (hcef) involving the NADPH dehydrogenase complex. *Plant Cell* **22,** 221–33 (2010).

4. Strand, D. D., Livingston, A. K., Satoh-cruz, M., Froehlich, J. E. & Maurino, V. G. Activation of cyclic electron flow by hydrogen peroxide in vivo. *Proc. Natl. Acad. Sci. U. S. A.* **112,** 5539–5544 (2015).

5. Sacksteder, C. A & Kramer, D. M. Dark-interval relaxation kinetics (DIRK) of absorbance changes as a quantitative probe of steady-state electron transfer. *Photosynth. Res.* **66,** 145–58 (2000).